Effects of Vibrational Frequency Correlations on Two-Dimensional Infrared Spectra†

Nien-Hui Ge, Martin T. Zanni, and Robin M. Hochstrasser*

Department of Chemistry, University of Pennsylvania, Philadelphia, Pennsylvania 19104-6323

Received: May 9, 2001; In Final Form: September 4, 2001

The response functions needed for simulating and fitting two-dimensional infrared spectra are described including the distributions of vibrational frequency, anharmonicity, and coupling between vibrators. A simple method that does not involve explicit calculation is introduced to characterize the spectral line narrowing properties of each of the quantum paths contributing to 2D IR. It is shown that the 2D IR spectra need to be collected in both positive and negative frequency quadrants in order to optimize the information needed to evaluate these correlations. Two experimental examples of heterodyned 2D IR (acetone in ethylene glycol and acetylproline-ND_2 in D_2O) are described where the 2D IR spectra are obtained for both the conventional echo sequence of pulse delays and for the usually nonrephased signal. These two sets of spectra are quite different for both examples, as predicted. The latter exhibits an echo only when there is some anticorrelation between the relevant inhomogeneous distributions.

Introduction

A new form of two-dimensional infrared spectroscopy (2D IR) that is analogous to coherent multiple pulse NMR[1] has been reported recently.[2] Since then, there were applications to peptides[3,4] and to metal carbonyls.[5] In this technique, the IR pulses manipulate the vibrational coherences in a manner that is formally equivalent to the radio frequency pulse induced exchange of spin coherences commonly used in NMR. The network of spins whose spatial distributions and dynamics are measured in NMR experiments is replaced in 2D IR by a network of vibrators whose angular relations, spatial separations, and dynamics are measured. The spectra are obtained as in NMR by Fourier transformation along at least two of the time delay axes defining the sequence of pulses and the free decay of the generated field. With regards to exhibiting line narrowing and displaying the diagonal and mixed mode anharmonic couplings these 2D vibrational spectra are in some sense *optimized IR spectra*. They have been ascertained to have significant potential for determining structure, structural dynamics, and structural distributions of complex molecules.[2−6] In this paper, we will show that the 2D IR method also divulges essential characteristics of the correlations between structural fluctuations associated with different vibrators in the network.

The prefix of 2D, 3D, or multidimensional has been used to mean many different things. In the present work, "multidimensional" is taken to mean the same as it does in NMR[1] where the terminology arose, namely, it is the complex spectrum of two or more freely decaying fields spread out into two or more frequency dimensions conjugate to the experimentally controllable time intervals characterizing the pulse sequence. This is the definition for a multiple pulse Fourier transform method. Two-dimensional measurements related to this definition have been reported previously for paramagnetic resonance spectroscopy of radicals,[7−9] for optical resonances of dyes,[10] for higher order Raman effects of liquids,[11] as well as for 2D IR spectroscopy[2−5] which we refer to as IR−COSY and forms the subject of this paper. However, other forms of 2D IR, such as the original double resonance[12,13] or pump/probe methods,[14] are also heterodyned although the signals does not contain the imaginary parts of the IR−COSY spectra. Fourier transform spectral interferometry of photon echoes of semiconductors was also reported.[15]

The heterodyned stimulated photon echo signal, which is at the basis of 2D IR, arises from overlapping the field generated by three phase locked IR pulses with a fourth IR pulse. The origin of this freely decaying oscillatory echo field for a particular set of pulse delays between the three phase locked IR pulses is usually represented by a set of Feynman diagrams or paths signifying the excitation of and transfer between various vibrational populations and coherences. The number of paths is limited by the rotating wave approximation. The pathways giving rise to the echo are often referred to as rephasing diagrams. These are the processes that would result in the rephasing of any induced dipoles that are present in the inhomogeneous distribution of vibrational frequencies. Other Feynman pathways, corresponding to different time orderings of the pulses, do not give the echo and have often been referred to as nonrephasing diagrams.[16] We shall show that the foregoing traditional picture of echoes applies strictly only to two-level systems. A vibrator or set of vibrators is in principle a multiple level system consisting of the set of vibrational quantum states of each of the coupled anharmonic oscillators. The system is therefore characterized by a number of Bohr frequencies, two in the case of a single oscillator, and $N(N^2 + N + 2)/2$ for N oscillators, assuming a third-order nonlinear optical process. We will show in this paper that it is essential to consider the correlations in the distributions associated with these Bohr frequencies to predict the rephasing and hence line narrowing properties of the system. This result is well-known in frequency domain nonlinear spectroscopy.[17] We will show that the pulse sequence alone does not predict whether there will be an echo

† This article was originally submitted for publication in the "Mitsuo Tasumi Festschrift".

* To whom correspondence should be addressed.

10.1021/jp011768o CCC: $22.00
Published on Web 10/31/2001

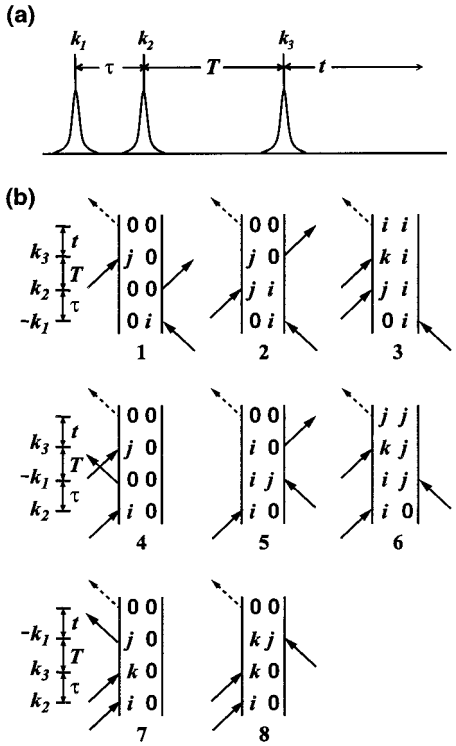

Figure 1. (a) Intervals between pulses for the three pulse photon echo experiment. (b) The Feynman diagrams contributing to the signal detected in the $-k_1 + k_2 + k_3$ direction for weakly coupled vibrators. Diagrams 1−3 and 4−6 correspond to the so-called "rephasing" and "nonrephasing" pathways, respectively. Diagrams 7−8 contribute only when the pulses are overlapped. Single quantum states are represented by *i* and *j* and two quantum states by *k*.

as was the case with two level systems and that line narrowed 2D IR spectra can be obtained from "nonrephasing" pathways. In previous work, we have shown how to incorporate the correlations of the frequency distributions of the fundamental and anharmonicity into the stimulated echo signals[18,19] of a single oscillator, but in this paper, we consider the more general questions relating to the echo fields and the 2D IR spectrum. We will illustrate by theoretical calculations the effects of these correlations on 2D IR spectra obtained for different pulse sequences. We will also present new experiments that illustrate major differences between the 2D IR spectra measured with the rephasing and nonrephasing pulse sequences and show that considerably more information will be obtained when heterodyned echo spectra are examined over the complete positive and negative frequency regimes.

Three Pulse Echoes and 2D IR

In third order 2D IR experiments, three phase-locked IR pulses with wavevectors k_1, k_2, and k_3 are incident on the sample in a sequence of τ and T as depicted in Figure 1a. The complex polarization $P(t;\tau,T)$ created for times t after the third pulse generates an in-quadrature electric field $E(t;\tau,T)$ that is then heterodyned by a local oscillator (LO) pulse and measured by a detector.[2−4] The heterodyned signal is a measure of $\mathrm{Re}[E(t;\tau,T)]$. When the time delay between the first two pulses, τ, is scanned in an experiment, the complex 2D IR spectrum $S(\omega_t,\omega_\tau)$ is obtained from the Fourier transform of the $\mathrm{Re}[E(t;\tau,T)]$, along t and τ, yielding frequency axes ω_t and ω_τ. Alternatively, one can scan the time delay between the second and third pulse, T, and obtain $S(\omega_t,\omega_T)$. When both τ and T are scanned, a 3D IR spectrum $S(\omega_t,\omega_\tau,\omega_T)$ can be obtained.

In this paper, we will consider a three-pulse photon echo experiment where the generated field emitted in the phase-matched direction $-k_1 + k_2 + k_3$ is measured by a detector. This field is made up of contributions from a number of Feynman paths. For a system of weakly coupled vibrators, the paths that survive the rotating wave approximation[20] are shown in Figure 1b. Here *i* represents the excited state of the system when one of the vibrators, *i*, is in its $v = 1$ state. When the system is doubly excited, it may involve an overtone state of a single vibrator *i* or a combination state of two singly excited vibrators *i* and *j*. These two quantum states labeled collectively as $k = i + j$ in Figure 1b correspond to overtone and combination states for $i = j$ and $i \neq j$, respectively. When the interaction of the set of vibrators with pulse k_1 occurs before the interaction with pulse k_2, rephasing diagrams 1−3 contribute to the signal. The coherence evolution involves frequencies of opposite signs during the τ and t period, as shown in the exponential factors in eq 1 below. When the ordering of pulses k_1 and k_2 is reversed, nonrephasing diagrams 4−6 contribute to the signal and the frequencies of the two coherences involved in the coherence evolution period have the same sign, as shown in eq 2 below. Note that both τ and T are defined as positive. The time τ is defined as the time separation between the peaks of k_1 and k_2. The time T is defined as the time separation between the peaks of k_2 and k_3 for rephasing diagrams 1−3, or between the peaks of k_1 and k_3 for nonrephasing diagrams 4−6.

The complex rephasing, E_R, and nonrephasing, E_{NR}, fields generated by an impulsively induced macroscopic polarization are given by

$$\begin{aligned}E_R(t;\tau,T) = \sum_{i\neq j}\langle a_i b_i c_i d_i\rangle e^{i\omega_i^0\tau}[F(0i|00|i0) + F(0i|ii|i0) - \\ F(0i|ii|i+i,i)\, e^{i\Delta_i^0 t}]e^{-i\omega_i^0 t} + \langle a_i b_i c_j d_j\rangle e^{i\omega_i^0\tau}[F(0i|00|j0) - \\ F(0i|ii|i+j,i)\, e^{i\Delta_{ij}^0 t}]e^{-i\omega_j^0 t} + \langle a_i b_j c_i d_j\rangle e^{i\omega_i^0\tau}[F(0i|ji|j0) - \\ F(0i|ji|i+j,i)\, e^{i\Delta_{ij}^0 t}]e^{-i\omega_{ji}^0 T - i\omega_j^0 t} - \\ \langle a_i b_i c_f d_f\rangle e^{i\omega_i^0\tau}F(0i|ii|j+j,i)\, e^{-i(2\omega_j^0 - \omega_i^0 - \Delta_j^0)t} - \\ \langle a_i b_j c_j d_f\rangle e^{i\omega_i^0\tau}F(0i|ji|j+j,i)\, e^{-i\omega_{ji}^0 T}e^{-i(2\omega_j^0 - \omega_i^0 - \Delta_j^0)t} - \\ \langle a_i b_j c_f d_i\rangle e^{i\omega_i^0\tau}F(0i|ji|i+i,i)\, e^{-i\omega_{ji}^0 T}e^{-i(\omega_i^0 - \Delta_i^0)t} \quad (1)\end{aligned}$$

$$\begin{aligned}E_{NR}(t;\tau,T) = \sum_{i\neq j}\langle a_i b_i c_i d_i\rangle e^{-i\omega_i^0\tau}[F(i0|00|i0) + F(i0|ii|i0) - \\ F(i0|ii|i+i,i)\, e^{i\Delta_i^0 t}]e^{-i\omega_i^0 t} + \langle a_i b_i c_j d_j\rangle e^{-i\omega_i^0\tau}[F(i0|00|j0) - \\ F(i0|ii|i+j,i)\, e^{i\Delta_{ij}^0 t}]e^{-i\omega_j^0 t} + \langle a_i b_j c_j d_i\rangle e^{-i\omega_i^0\tau}[F(i0|ij|i0) - \\ F(i0|ij|i+j,j)\, e^{i\Delta_{ij}^0 t}]e^{-i\omega_{ij}^0 T - i\omega_i^0 t} - \\ \langle a_i b_i c_f d_f\rangle e^{-i\omega_i^0\tau}F(i0|ii|j+j,i)\, e^{-i(2\omega_j^0 - \omega_i^0 - \Delta_j^0)t} - \\ \langle a_i b_j c_i d_f\rangle e^{-i\omega_i^0\tau}F(i0|ij|i+i,j)\, e^{-i\omega_{ij}^0 T}e^{-i(2\omega_i^0 - \omega_j^0 - \Delta_i^0)t} - \\ \langle a_i b_j c_f d_j\rangle e^{-i\omega_i^0\tau}F(i0|ij|j+j,j)\, e^{-i\omega_{ij}^0 T}e^{-i(\omega_j^0 - \Delta_j^0)t} \quad (2)\end{aligned}$$

Here, the mean values of the fundamental frequencies are ω_i^0, the overtones are at $2\omega_i^0 - \Delta_i^0$, the combination tones are at $\omega_i^0 + \omega_j^0 - \Delta_{ij}^0$, Δ_i^0 and Δ_{ij}^0 are mean values of diagonal and off-diagonal anharmonicities, respectively, and $\omega_{ij}^0 \equiv \omega_i^0 - \omega_j^0$. The implicitly time dependent polarization factors $\langle a_i b_j c_l d_m\rangle$ depend on: the polarization of the infrared pulses in the laboratory frame, indicated as *a*, *b*, *c*, and *d*; on the angles between these directions and the transition dipoles, indicated as *i*, *j*, *l*, and *m*, involved in the four time steps; and on the orientation dynamics[21] assumed to be independent of the

vibrational dynamics. The terms in the last three lines in eqs 1 and 2 have one or more transition dipoles that are forbidden in the harmonic approximation, such as $i \rightarrow j + j$, which is zero in the extreme weak coupling approximation when i and j represent different oscillators. These transitions have polarization factors with terms labeled "*f*" for "forbidden" because the orientations of their transition dipoles depend on the details of how the oscillators are coupled. We will omit these forbidden terms in the following model calculations. The $F(ij|kl|mn)$ factors, where the three pairs of indices taken from left to right correspond to the coherences created by the first, second, and third pulses, contain the magnitudes of the transition dipole moments and the dynamics during the τ, T, and t periods, which in general include population relaxation, dephasing, and spectral diffusion. For example, $F(0i|ji|i + j,i)$ contains the ensemble averaged dynamical part of diagram 3 of Figure 1b when $k = i + j$ and the product of transition dipole magnitudes $\mu_i\mu_j\mu_{i+j,i}\mu_{i,i+j}$. For simplicity, we will make the assumptions of $\mu_{i,i+i} = \sqrt{2}\mu_i$ and $\mu_{i,i+j} = \mu_j$ throughout the rest of the paper. If the magnitudes deviate from these assumptions, the transition dipoles needed in the process can be easily included by inspecting the indices of the $F(ij|kl|mn)$ factors.

In the case of $T = 0$, the double Fourier transform of the real parts of eqs 1 and 2 along t and τ gives a complex 2D spectrum $S(\omega_t,\omega_\tau)$. For example, the fourth term of eqs 1 or 2 involves $0i$ (or $i0$) and $j0$ coherences during the τ and t periods. In the approximation of Bloch dynamics, where the vibrational dephasing is in the motional narrowing limit and there exists a static inhomogeneous distribution of frequencies, the $F(ij|kl|mn)$ factors in these terms become functions of the total dephasing rates of the level pairs listed and the deviations of the frequencies from their mean values. Because Fourier transformation is linear, we can first Fourier transform the time response to the frequency domain and then average the complex 2D spectrum over the inhomogeneous distribution. The contribution of these terms to the 2D spectrum is then

$$\left\langle \frac{\langle a_i b_i c_j d_j\rangle \mu_i^{\,2}\mu_j^{\,2}}{[\mp\omega_i - \omega_\tau - i\gamma_{0i}][\omega_j - \omega_t - i\gamma_{0j}]} \right\rangle + \text{complex conjugate}, \tag{3}$$

where $-$ and $+$ in $\mp$ correspond to the rephasing and nonrephasing terms, respectively, the outer $\langle\cdots\rangle$ represents averaging over the inhomogeneous frequency distribution, and γ_{ij} are the total dephasing rates of the level pairs listed. The rephasing terms are located in the second and fourth quadrant of the 2D spectrum (Figure 2a) of ω_τ versus ω_t. These two spectra contain identical information because they come from terms that are complex conjugates. Likewise, the nonrephasing terms determine the spectra obtained in the first and third quadrant, and the two quadrants also contain identical information. For a single vibrator, only the first three terms of eqs 1 and 2 for the generated fields are needed.

Note that when the pulse widths are finite, the nonlinear responses need to be convoluted with the pulse width in order to give the complex field. During the time when the pulses are overlapped, in addition to the rephasing and nonrephasing diagrams discussed above, diagrams with other time ordering [7−8 in Figure 1b] will also contribute to the signal. The nonlinear response $R(t;\tau,T)$ from these diagrams is given by

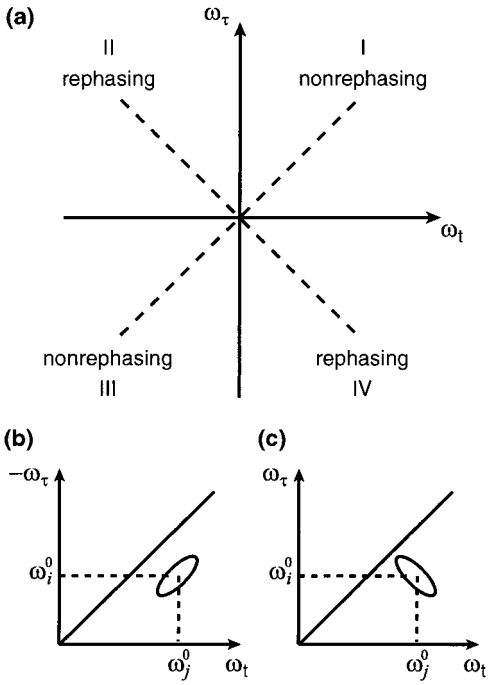

Figure 2. (a) Four frequency quadrants in a 2D IR spectrum. Rephasing terms are located in quadrants II and IV, and nonrephasing terms are located in quadrants I and III. Dashed lines indicate the diagonals. Line-narrowing properties of eq 3 are shown for the rephasing term at $c = 1$ (b) and nonrephasing term at $c = -1$ (c).

$$\begin{aligned} R(\tau;t,T) = i\sum_{i\neq j} \mathrm{e}^{-i\omega_i{}^0\tau}\{&\langle a_i b_i c_i d_j\rangle[F(i0|i + i,0|i0) - \\ &F(i0|i + i,0|i + i,i)\ \mathrm{e}^{i\Delta_i{}^0 t}]\mathrm{e}^{-i(2\omega_i{}^0-\Delta_i{}^0)T}\mathrm{e}^{-i\omega_i{}^0 t} + \\ &\langle a_i b_j c_i d_j\rangle[F(i0|i + j,0|j0) - \\ &F(i0|i + j,0|i + j,i)\ \mathrm{e}^{i\Delta_{ij}{}^0 t}]\mathrm{e}^{-i(\omega_i{}^0+\omega_j{}^0-\Delta_{ij}{}^0)T}\mathrm{e}^{-i\omega_j{}^0 t} + \\ &\langle a_i b_j c_j d_i\rangle[F(i0|i + j,0|i0) - \\ &F(i0|i + j,0|i + j,j)\ \mathrm{e}^{i\Delta_{ij}{}^0 t}]\mathrm{e}^{-i(\omega_i{}^0+\omega_j{}^0-\Delta_{ij}{}^0)T}\mathrm{e}^{-i\omega_i{}^0 t} + \\ &\mathrm{e}^{-i(2\omega_i{}^0-\Delta_i{}^0)T}[\langle a_i b_i c_f d_j\rangle F(i0|i + i,0|j0)\ \mathrm{e}^{-i\omega_j{}^0 t} - \\ &\langle a_i b_i c_j d_f\rangle F(i0|i + i,0|i + i,j)\ \mathrm{e}^{-i(2\omega_i{}^0-\omega_j{}^0-\Delta_i{}^0)t}] + \\ &\mathrm{e}^{-i(2\omega_j{}^0-\Delta_j{}^0)T}[\langle a_i b_f c_i d_f\rangle F(i0|j + j,0|i0)\ \mathrm{e}^{-i\omega_i{}^0 t} - \\ &\langle a_i b_f c_i d_f\rangle F(i0|j + j,0|j + j,i)\ \mathrm{e}^{-i(2\omega_j{}^0-\omega_i{}^0-\Delta_j{}^0)t} + \\ &\langle a_i b_f c_j d_j\rangle F(i0|j + j,0|j0)\ \mathrm{e}^{-i\omega_j{}^0 t} - \\ &\langle a_i b_f c_j d_j\rangle F(i0|j + j,0|j + j,j)\mathrm{e}^{-i(\omega_j{}^0-\Delta_j{}^0)t}]\}. \end{aligned} \tag{4}$$

The frequencies of the two coherences involved in the evolution period τ (defined in Figure 1b, 7−8) and t have the same sign, just like the nonrephasing terms in eq 2, but the frequencies during the T period involve overtone and combination band frequencies. These $F(ij|kl|mn)$ terms can also be modeled by the same theory developed below. Because these diagrams only contribute when the pulses are overlapped and vibrational coherences often decay on a much longer time scale than the pulse widths, we will consider impulsive excitations and omit their contributions.

Qualitative Model of the Line Narrowing Properties of 2D IR Spectroscopy

We first outline a simple method,[17] which does not involve explicit calculation, whereby the line narrowing property of a term like eq 3 can be quickly evaluated. It assumes, *without*

loss of generality in regard to this objective, that the inhomogeneous distribution is a Lorentzian $G(x) = \sigma/[\pi(x^2 + \sigma^2)]$. First, the frequencies are written in terms of the deviations x and y from their mean values, so that $\omega_i = \omega_i^0 + x$ and $\omega_j = \omega_j^0 + cy$. In the special cases where $x = y$ and c is $+1$ or -1, the results describe strictly correlated and anticorrelated distributions, respectively, then the average in eq 3 over x can be performed analytically by applying the residue theorem. When $c = +1$ both poles exhibited in the nonrephasing choice of signs in eq 3 are above the real axis on the complex plane, as is one of the poles from $G(x)$. The only pole below the real axis is at $x = -i\sigma$, so all of the spectral terms contain the inhomogeneous width of $G(x)$ and are therefore not line narrowed. On the contrary, if the rephasing part of eq 3 is chosen, the pole involving ω_i is shifted below the real axis resulting in a residue that contributes a line narrowed spectrum. If we choose $c = -1$, the line narrowing occurs only in the nonrephasing spectrum. In summary, if the two residues in equations of the type 3 are on the opposite sides of the real axis, the spectrum is line narrowed, otherwise it is not. When the distributions are correlated, the narrowed peak occurs at $\omega_i^0 + \omega_\tau = \omega_j^0 - \omega_t$ as shown in Figure 2a,b, but when they are anticorrelated, the peak is along $\omega_i^0 - \omega_\tau = -(\omega_j^0 - \omega_t)$ as in Figure 2a,c. The conventional terms "nonrephasing diagram" and "rephasing diagram" are no longer descriptive when the correlation coefficient differs from ± 1. The occurrence of an echo is determined by whether the inhomogeneous distribution present during the interval t can rephase, which in turn depends on the correlation between the distributions involved in the t and τ evolution. The simple method outlined above can be applied to a system having arbitrary correlation coefficients by choosing deviations that are linear combinations of x and y,[17] but we will not pursue this approach here.

To facilitate the comparison between the rephasing and nonrephasing parts of the spectrum, we will from now on focus on the fourth and first quadrants and plot the fourth quadrant in its mirror reflection about the abscissa, so that the diagonals of spectra in the two quadrants are parallel to each another. As discussed above and illustrated in Figure 2b,c, the shapes of the rephasing and nonrephasing spectra very much depend on the correlation between the inhomogeneous frequency distributions of the two coherences involved. When the same coherence is involved in both the τ and t periods, there is strict correlation, and only the rephasing part shows line narrowing. This corresponds to the two-pulse photon echo signals of a simple two-level system and the usual concept that a photon echo is a line narrowing technique actually refers to the rephasing part of the spectrum. When two different coherences associated with one oscillator are involved, the degree of line narrowing in the rephasing and nonrephasing spectra depends on the correlation between the fluctuations of the $1-2$ and $0-1$ transitions, so that the frequency correlation between the anharmonicity Δ_i and ω_i determines the spectral line shape. When coherences on different vibrators are involved, the frequency correlation between the distributions of the two vibrators is revealed. Therefore, 2D IR spectroscopy has the capability to reveal the frequency correlations within the same vibrator or between vibrators on different sites. It provides detailed information on the fluctuation of intra- and intermolecular potentials that is not readily available from other techniques applicable in solutions.

Nonlinear Responses Including Correlations

In this section, we model the dynamics of the system and include correlations. The vibrational relaxation between level pairs is neglected, the population relaxation of the ith level is taken into account phenomenologically by a decay time T_1^i, and we assume that the system-bath coupling is governed by stochastic processes that follow Gaussian statistics. Omitting the forbidden terms, the $F(ij|kl|mn)$ factors in eqs 1 and 2 can be written down immediately as

$$F\left(\begin{Bmatrix}0i\\i0\end{Bmatrix}\middle|ii\middle|i0\right) = F\left(\begin{Bmatrix}0i\\i0\end{Bmatrix}\middle|00\middle|i0\right) = \mu_i^4 \exp\left[-\frac{1}{2T_1^i}(\tau + 2T + t) - g_{ii}(\tau) \pm g_{ii}(T) - g_{ii}(t) \mp g_{ii}(\tau + T) \mp g_{ii}(T + t) \pm g_{ii}(\tau + T + t)\right] \quad (5)$$

$$F\left(\begin{Bmatrix}0i\\i0\end{Bmatrix}\middle|ii\middle|i+i,i\right) = 2F\left(\begin{Bmatrix}0i\\i0\end{Bmatrix}\middle|ii\middle|i0\right) \exp\left[-\frac{t}{2T_1^{i+i}} - g_{\Delta_i\Delta_i}(t) \mp g_{i\Delta_i}(T) + 2g_{i\Delta_i}(t) \pm g_{i\Delta_i}(\tau + T) \pm g_{i\Delta_i}(T + t) \mp g_{i\Delta_i}(\tau + T + t)\right] \quad (6)$$

$$F\left(\begin{Bmatrix}0i\\i0\end{Bmatrix}\middle|00\middle|j0\right) = \mu_i^2\mu_j^2 \exp\left[-\frac{\tau}{2T_1^i} + \frac{T}{T_1^i} + \frac{t}{2T_1^j} - g_{ii}(\tau) \pm g_{ij}(T) - g_{jj}(t) \mp g_{ij}(\tau + T) \mp g_{ij}(T + t) \pm g_{ij}(\tau + T + t)\right] \quad (7)$$

$$F\left(\begin{Bmatrix}0i\\i0\end{Bmatrix}\middle|ii\middle|i+j,i\right) = F\left(\begin{Bmatrix}0i\\i0\end{Bmatrix}\middle|00\middle|j0\right) \exp\left[-\frac{t}{2T_1^{i+j}} - \frac{t}{2T_1^i} + \frac{t}{2T_1^j}\right] \quad (8)$$

$$F(0i|ji|j0) = \mu_i^2\mu_j^2 \exp\left[-\left(\frac{\tau + T}{2T_1^j} + \frac{T + t}{2T_1^j}\right) - g_{ij}(\tau) + g_{ij}(T) - g_{ij}(t) - g_{ii}(\tau + T) - g_{jj}(T + t) + g_{ij}(\tau + T + t)\right] \quad (9)$$

$$F(0i|ji|i+j,i) = F(0i|ji|j0) \exp\left[-\frac{t}{2T_1^{i+j}} - \frac{t}{2T_1^i} + \frac{t}{2T_1^j}\right] \quad (10)$$

$$F(i0|ij|i0) = \mu_i^2\mu_j^2 \exp\left[-\left(\frac{\tau + T + t}{2T_1^i} + \frac{t}{2T_1^i}\right) - g_{ij}(\tau) - g_{jj}(T) - g_{ij}(t) + g_{ij}(\tau + T) + g_{ij}(T + t) - g_{ii}(\tau + T + t)\right] \quad (11)$$

$$F(i0|ij|i+j,j) = F(i0|ij|i0) \exp\left[-\frac{t}{2T_1^{i+j}} - \frac{t}{2T_1^j} + \frac{t}{2T_1^i}\right] \quad (12)$$

Here the line shape functions[22] are generally defined as

$$g_{ab}(t) = \int_0^t d\tau_1 \int_0^{\tau_1} d\tau_2 \langle \delta\omega_a(\tau_2)\delta\omega_b(0)\rangle \quad (13)$$

where $\langle \delta\omega_a(\tau_2)\delta\omega_b(0)\rangle$ is the correlation function of the vibrational frequency fluctuations, $\delta\omega_a(t)$ and $\delta\omega_b(t)$, about their mean values. The line shape functions included in this model are $g_{ii}(t)$, $g_{\Delta_i\Delta_i}(t)$, $g_{i\Delta_i}(t)$, and $g_{ij}(t)$, corresponding to autocorrelation functions $\langle \delta\omega_i(\tau_2)\delta\omega_i(0)\rangle$ and $\langle \delta\Delta_i(\tau_2)\delta\Delta_i(0)\rangle$ and cross-correlation functions $\langle \delta\omega_i(\tau_2)\delta\Delta_i(0)\rangle$ and $\langle \delta\omega_i(\tau_2)\delta\omega_j(0)\rangle$, respectively. The fluctuation in the off-diagonal anharmonicity, $\delta\Delta_{ij}(t)$, is ignored here, although it can be incorporated in a similar way and we will discuss its effects in the next section. Equations 5−12 along with (1) and (2) define the third-order response functions of a set of pairwise correlated oscillators assuming no fluctuations in the off-diagonal anharmonicity.

These response functions can be used for simulation of many types of third-order infrared spectroscopy, including pump−probe 2D IR experiments;[12−14] two pulse[23] or three pulse[24,25] photon echo experiments with integrated, frequency-resolved,[18,26] time-gated, or heterodyned[2−5] detection; and transient grating[6] experiments. Terms in eq 4, such as $F(i0|i+j,0|i+j,i)$, which only appear near $\tau = 0$ are not considered in eqs 5−12. In the following, we will focus on 2D IR spectra obtained from heterodyned three pulse photon echo with $T = 0$.

Nonlinear Responses using Bloch Dynamics

In the case of a strict separation of time scales of homogeneous and inhomogeneous broadening, i.e. Bloch dynamics, the line shape functions $g_{ii}(t)$, $g_{\Delta_i\Delta_i}(t)$, $g_{i\Delta_i}(t)$, and $g_{ij}(t)$ become $(\Gamma_i t + \sigma_i^2 t^2/2)$, $(\Gamma_{\Delta_i} t + \sigma_{\Delta_i}^2 t^2/2)$, $f_i\sigma_i\sigma_{\Delta_i} t^2/2$, and $c_{ij}\sigma_i\sigma_j t^2/2$, respectively, where Γ_i is the motionally narrowed pure dephasing rate of the 0−1 transition for vibrator i, Γ_{Δ_i} characterizes the motionally narrowed part of the diagonal anharmonicity fluctuations, and σ_i and σ_{Δ_i} characterize the widths of the Gaussian inhomogeneous distributions of the 0−1 transition and diagonal anharmonicity, respectively. The statistical correlation coefficients f_i and c_{ij} are defined as $\langle\delta\omega_i\cdot\delta\Delta_i\rangle/(\sigma_i\sigma_{\Delta_i})$, and $\langle\delta\omega_i\cdot\delta\omega_j\rangle/(\sigma_i\sigma_j)$, respectively. Under these assumptions and setting $T = 0$, the $F(ij|kl|mn)$ factors in eqs 5−12 become

$$F\left(\begin{Bmatrix}0i\\i0\end{Bmatrix}\middle|00\middle|i0\right) = F\left(\begin{Bmatrix}0i\\i0\end{Bmatrix}\middle|ii\middle|i0\right) = \mu_i^4 \exp\left[-\frac{1}{2T_1^{\,i}}(\tau+t) - \Gamma_i(\tau+t) - \frac{1}{2}\sigma_i^2(\tau \mp t)^2\right] \quad (14)$$

$$F\left(\begin{Bmatrix}0i\\i0\end{Bmatrix}\middle|ii\middle|i+i,i\right) = 2F\left(\begin{Bmatrix}0i\\i0\end{Bmatrix}\middle|ii\middle|i0\right) \exp\left[-\left(\frac{1}{2T_1^{\,i+i}} + \Gamma_{\Delta_i}\right)t + f_i\sigma_i\sigma_{\Delta_i}t(t \mp \tau) - \frac{1}{2}\sigma_{\Delta_i}^2 t^2\right] \quad (15)$$

$$F\left(\begin{Bmatrix}0i\\i0\end{Bmatrix}\middle|00\middle|j0\right) = \mu_i^2\mu_j^2 \exp\left[-\left(\frac{1}{2T_1^{\,i}} + \Gamma_i\right)\tau - \left(\frac{1}{2T_1^{\,j}} + \Gamma_j\right)t - \frac{1}{2}\sigma_i^2\tau^2 - \frac{1}{2}\sigma_j^2 t^2 \pm c_{ij}\sigma_i\sigma_j\tau t\right] \quad (16)$$

$$F\left(\begin{Bmatrix}0i\\i0\end{Bmatrix}\middle|ii\middle|i+j,i\right) = F\left(\begin{Bmatrix}0i\\i0\end{Bmatrix}\middle|00\middle|j0\right) \exp\left[-\frac{t}{2T_1^{\,i+j}} - \frac{t}{2T_1^{\,i}} + \frac{t}{2T_1^{\,j}}\right] \quad (17)$$

$$F(0i|ji|j0) = F(0i|00|j0) \quad (18)$$

$$F(0i|ji|i+j,i) = F(0i|ii|i+j,i) \quad (19)$$

$$F(i0|ij|i0) = F(i0|ii|i0)\,(\mu_j^2/\mu_i^2) \quad (20)$$

$$F(i0|ij|i+j,j) = F(i0|ij|i0) \exp\left[-\frac{t}{2T_1^{\,i+j}} - \frac{t}{2T_1^{\,j}} + \frac{t}{2T_1^{\,i}}\right]. \quad (21)$$

For a single vibrator, only eqs 14 and 15 and the first three terms of (1) and (2) are needed. The rephasing part for a single vibrator derived here is the same as that in ref 18 even though a different method of derivation has been employed.

We performed model calculations using eqs 14−21 along with (1) and (2) to illustrate the effects of correlations among the various frequency distributions on the 2D spectra. All calculations were done under the assumptions of $(T_1^{\,i+i})^{-1} = 2(T_1^{\,i})^{-1}$ and $(T_1^{\,i+j})^{-1} = (T_1^{\,i})^{-1} + T_1^{\,j})^{-1}$. These relations between T_1 are what one may expect from a harmonic oscillator linearly coupled to bath modes. We have also assumed that the diagonal anharmonicity has no fast fluctuations so that $\Gamma_{\Delta_i} = 0$. The parameters were set to the values, $T_1^{\,i} = 2.5$ ps, $\Delta_i^0 = 16$ cm^{-1}, and $\sigma_{\Delta_i} = 1.6$ cm^{-1}, unless otherwise mentioned. The values of $T_1^{\,i}$ and Δ_i^0 are typical for C═O vibrations. The fluctuation σ_{Δ_i} was taken to be one tenth Δ_i^0. Such fluctuations in the anharmonicity are justified on the basis of spectroscopic results. For example it has been found that the anharmonicity constant of C═O vibrations of acetophenone and benzophenone can change by as much as 40% in different solvents, ranging from CCl_4, CH_2Cl_2, CH_2Br_2 to $CHCl_3$.[27] A 30% difference in the anharmonicity of the C−O stretch is found for CH_3O in a supersonic jet[28] and in an argon matrix.[29] A 5% or 15% difference in the anharmonicity of HF stretch is found for gas-phase HF in various hydrogen-bonded complexes.[30] From these examples, we can expect that different solvent configurations could introduce a significant distribution of anharmonicities.

The calculated absolute value 2D spectra, $|S(\omega_t,\omega_\tau)|$, for a single vibrator i are shown in Figure 3. In the homogeneous limit, the rephasing and nonrephasing parts of the power spectrum have the same shapes and intensities and are unaffected by correlation (Figure 3a). The 2D line shape is symmetric with respect to the horizontal axis with the wings extending more in the ω_τ direction than in the ω_t direction. This line shape results from summing two 2D spectra which are displaced by the diagonal anharmonicity Δ_i^0 in the ω_t direction and are opposite in sign. The line widths of the two 2D spectra as determined by eqs 14 and 15 are the same along the ω_τ direction but different along the ω_t direction because the 1−2 transition in general possesses a faster dephasing rate than the 0−1 transition due at least in part to the different population decay contributions. As the inhomogeneous width increases, the line shape and intensity differences between the rephasing and nonrephasing spectra increases, and correlation begins to affect the spectra. Figure 3b−d illustrates the situation for large inhomogeneous broadening with $f_i = 1$, 0, and −1, respectively. The 2D spectra plotted here contain contributions from eqs 14 and 15, and their individual contributions will be summarized below. The 2D line shape from eq 14 is strongly elongated along the diagonal axis of the rephasing spectrum, showing an inhomogeneously broadened width and is line-narrowed when slicing through the antidiagonal. There is, however, no line narrowing in the nonrephasing spectrum, and hence, the peak height is significantly reduced. On the other hand, the 2D line shapes of eq 15 have additional dependence on the frequency correlation between the 0−1 and 1−2 transitions and on the difference in the dephasing rates. For zero correlation, the axis of elongation in the rephasing spectrum lies along the diagonal if the two transitions have similar total dephasing rates. Positive and negative correlations make the elongation axis lie at an angle counterclockwise and clockwise from that of zero correlation, respectively. The nonrephasing spectrum exhibits no line-narrowing as before, but the line width along the ω_t axis, compared to that of the zero correlation case, changes from being narrower to broader when the correlation changes from positive to negative. Figure 3b−d is the results of the composite effects from eqs 14 and 15.

For the case of two vibrators, we focus the discussion on the effects of cross correlation between vibrators, i.e., the effects of c_{ij}, and choose the example of correlation coefficients $f_i = f_j = 0$. This implies that we have assumed that the fluctuations

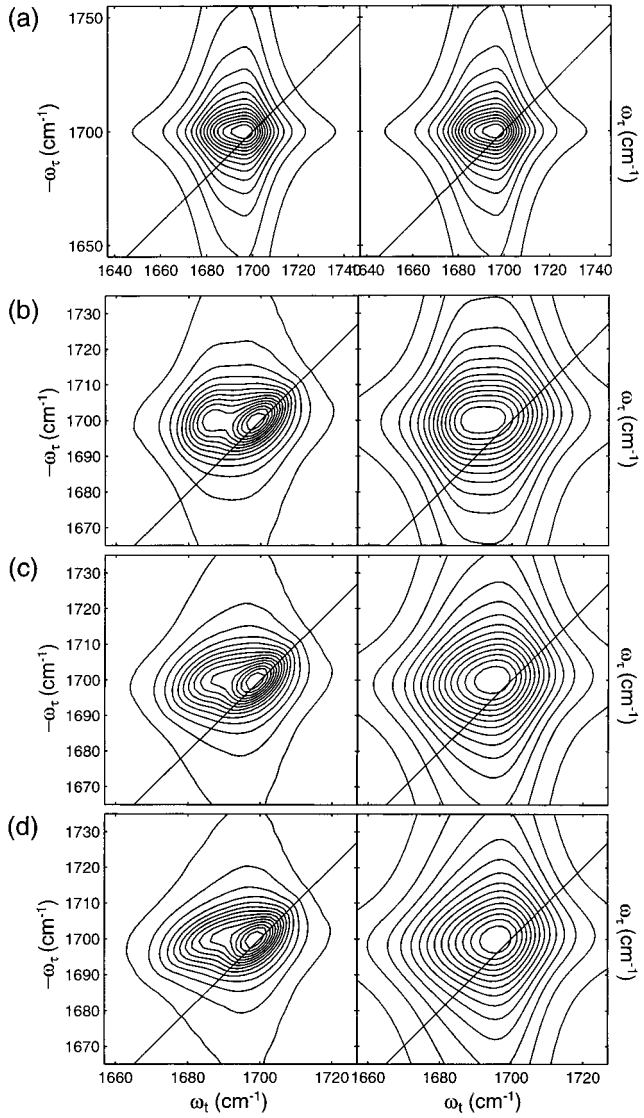

Figure 3. Calculated absolute value 2D IR spectra for a single vibrator at $\omega_i^0 = 1700$ cm^{-1}. Rephasing spectra are plotted on the left and nonrephasing spectra for the same parameters on the right. The dynamics is in the homogeneous limit for (a) with $\Gamma_i = 6.4$ cm^{-1} and $\sigma_i = 0$, and dominated by static inhomogeneous broadening for (b)−(d) with $\Gamma_i = 1.6$ cm^{-1} and $\sigma_i = 4.3$ cm^{-1}. Correlation coefficent $f_i = 1$, 0, and -1 for b, c, and d, respectively. All spectra are normalized by the peak maximum and plotted with 15 evenly spaced contour lines spanning from 0 to 1. The actual intensity of the peak maximum of the nonrephasing spectrum is 1, 0.42, 0.38, and 0.35 times that of the rephasing spectrum for a−d, respectively.

of the diagonal anharmonicities are not correlated to the corresponding 0−1 transition frequencies. Figure 4 parts a−c illustrates the rephasing and nonrephasing absolute value 2D spectra for two coupled vibrators with $c_{ij} = 1$, 0, and -1, respectively. The case of $c_{ij} = 0$ may be applicable to cases such as the dipeptides that have been studied[4,31] where the two coupled vibrators are at different ends of the peptide and can each independently interact with surrounding solvents. In this example, we illustrate the situation for large inhomogeneous broadening, assuming that the two vibrators have the same dynamical parameters and transition dipole strength and their frequencies are separated by 40 cm^{-1}. We have assumed that the coupling between the two vibrators is $\beta_{ij}^0 = 6$ cm^{-1}, giving rise to an electrostatic contribution to Δ_{ij}^0 of 1.4 cm^{-1} (see next section for a relation between β_{ij} and Δ_{ij}). The line shape and intensity of the cross-peaks clearly depend on the frequency correlation between the two vibrators. In the rephasing spectra, the cross-peaks are pronounced and line-narrowed for positive correlation (Figure 4a) but broadened and diminished as the correlation becomes zero and negative (Figure 4 parts c and e). On the contrary, in the nonrephasing spectra, the cross-peaks are line-narrowed in the direction perpendicular to that in the rephasing spectra for negative correlation (Figure 4f), but broadened as the correlation becomes zero or positive (Figure 4 parts d and b). The results imply that the coupling strength between vibrators cannot be determined merely based on the cross-peak intensities in a rephasing spectrum where the low intensities may result from negative correlations rather than from small coupling. Measuring rephasing and nonrephasing spectra separately is expected to provide more complete information on coupling and correlation.

In addition to providing information on correlation, comparison of the rephasing and nonrephasing spectra also provides information on the underlying vibrational dynamics. Figure 5 shows absolute value 2D spectra for two coupled vibrators having different dynamics. The parameters are chosen such that the transitions of the vibrator with higher fundamental frequency are dominated by homogeneous broadening and those of the lower frequency one are dominated by inhomogeneous broadening, but their linear spectra have the same widths and heights. The diagonal peaks differ dramatically in their line shapes and intensities, demonstrating that 2D spectra are highly sensitive to the underlying dynamics that make up the linear spectra.

In general, the inhomogeneous frequency distribution of a vibrator need not be a singly peaked function. For example, in the presence of multiple conformations where vibrators in different conformers exhibit different fundamental frequencies, one can think of the system as a sum of multiple uncoupled and independent vibrators, each having a distinct central frequency and the associated inhomogeneous distribution. Alternatively, one can think of the system as a single vibrator with a multiple peaked frequency distribution function. Figure 6a shows absolute value 2D spectra for the case of two vibrators with identical parameters except for fundamental frequencies. The separation in frequencies is less than the line width, so that the two peaks merge into a single peak in the rephasing spectrum. In this situation, it is not straightforward to tell the existence of two vibrators. The ability to distinguish the underlying spectral features can be improved by examining the nonrephasing spectrum where a valley may appear between two peaks. The reason for this improvement is that the nodal lines in the real and imaginary parts of the complex spectra are perpendicular to the diagonal in the nonrephasing spectra [shown for one of the vibrators in Figure 6 parts b and c], giving rise to destructive interference in the overlapping region between vibrators. The nodal lines are parallel to the diagonal in the rephasing spectra, resulting in constructive interference between vibrators. This example shows that if the spectra are measured in both quadrants the information content is made more evident.

Effects of Fluctuations in the Off-Diagonal Anharmonicity

For this discussion, we will assume the vibrators as electrostatically coupled separated systems. In the weak coupling limit where the frequency separations between the uncoupled modes are large compared with the individual couplings, β_{ij}, the off-diagonal anharmonicity can be calculated from perturbation theory as $\Delta_{ij} = 4\Delta_i\beta_{ij}^2/(\omega_i - \omega_j)^2$.[32] The fluctuation of the off-diagonal anharmonicity about its mean value is then given by $\delta\Delta_{ij} = \Delta_{ij}^0[\delta\Delta_i/\Delta_i^0 + 2\delta\beta_{ij}/\beta_{ij}^0 - 2(\delta\omega_i - \delta\omega_j)/(\omega_i^0 - \omega_j^0)]$. The

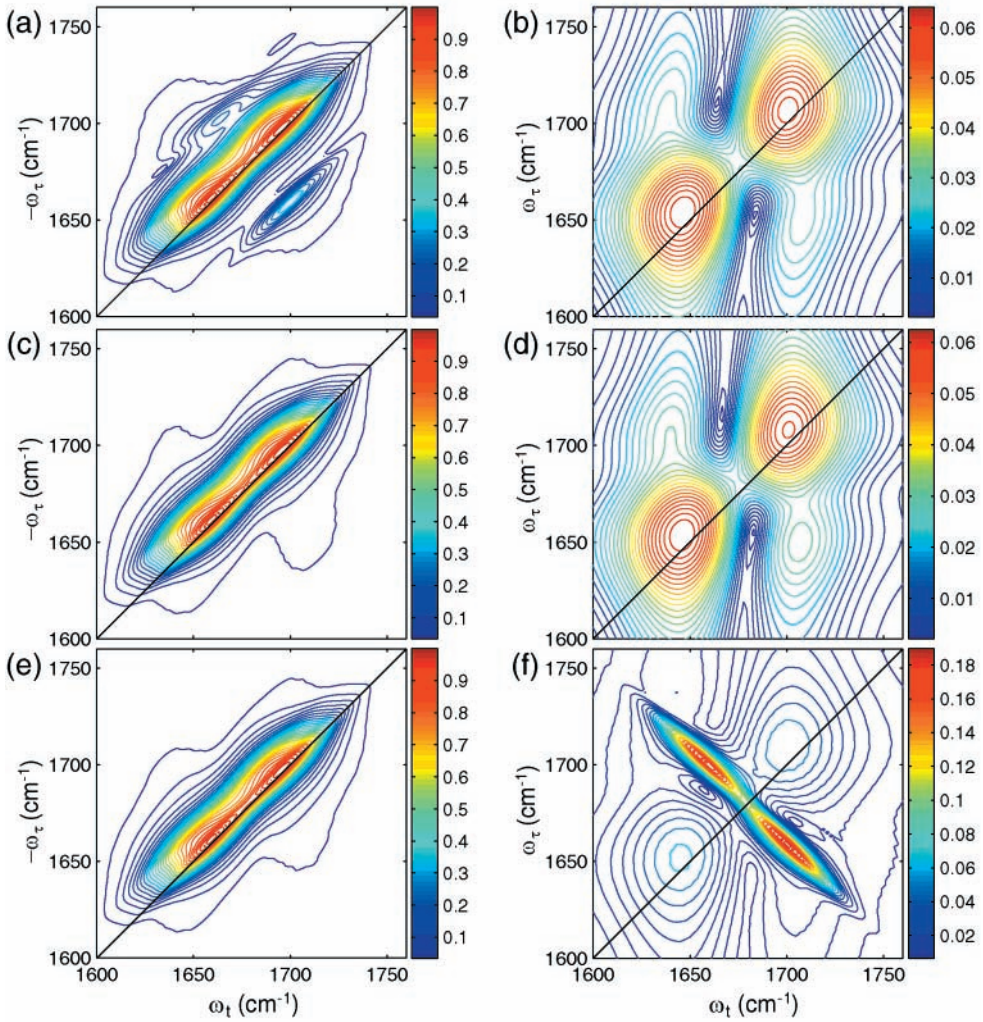

Figure 4. Calculated absolute value 2D spectra for two coupled vibrators at $\omega_i^0 = 1700$ cm^{-1} and $\omega_j^0 = 1660$ cm^{-1}. The dynamical parameters are identical for the two vibrators with $\Gamma_i = 1.6$ cm^{-1} and $\sigma_i = 15$ cm^{-1}. Frames a, c, and e are rephasing spectra with correlation coefficent $c_{ij} = 1$, 0, and -1, respectively. Frames b, d, and f are the corresponding nonrephasing spectra.

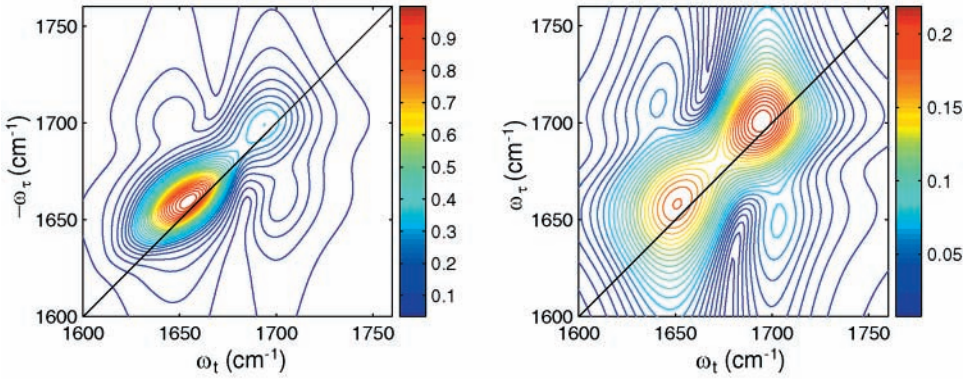

Figure 5. Calculated absolute value 2D spectra for two coupled vibrators at $\omega_i^0 = 1700$ cm^{-1} and $\omega_j^0 = 1660$ cm^{-1} with $f_i = 0$ and $c_{ij} = 0$. The dynamical parameters for the two vibrators are $\Gamma_i = 12.3$ cm^{-1}, $\sigma_i = 6.1$ cm^{-1}, $\Gamma_j = 3.8$ cm^{-1}, and $\sigma_j = 11.8$ cm^{-1}. Left: rephasing spectrum. Right: nonrephasing spectrum.

inclusion of $\delta\Delta_{ij}$ introduces into eqs 17, 19, and 21 additional exponential factors that contain the line shape functions $g_{i\Delta_{ij}}(t)$, $g_{j\Delta_{ij}}(t)$, and $g_{\Delta_{ij}\Delta_{ij}}(t)$, corresponding to cross-correlation functions $\langle\delta\omega_i(\tau_2)\delta\Delta_{ij}(0)\rangle$ and $\langle\delta\omega_j(\tau_2)\delta\Delta_{ij}(0)\rangle$ and autocorrelation function $\langle\delta\Delta_{ij}(\tau_2)\delta\Delta_{ij}(0)\rangle$. If $\delta\beta_{ij} = 0$ is assumed, these line shape functions can be expressed as linear combinations of $g_{i\Delta_i}(t)$, $g_{\Delta_i\Delta_i}(t)$, $g_{ii}(t)$, and $g_{ij}(t)$ derived in the previous section times the factors Δ_{ij}^0/Δ_i^0 or $\Delta_{ij}^0/(\omega_i^0 - \omega_j^0)$ to the first or second power. The net effect is to introduce exponentially growing or decaying factors into eqs 17, 19, and 21, depending on the sign of $(\omega_i^0 - \omega_j^0)$. Therefore, the overall contributions from eqs. 16−21 are not equivalent for cross-peaks appearing on the opposite sides of the diagonal, resulting in asymmetry about the diagonal in the 2D IR spectra. This effect may contribute to the asymmetry that has been observed experimentally.[4] The line narrowing properties discussed in the previous section

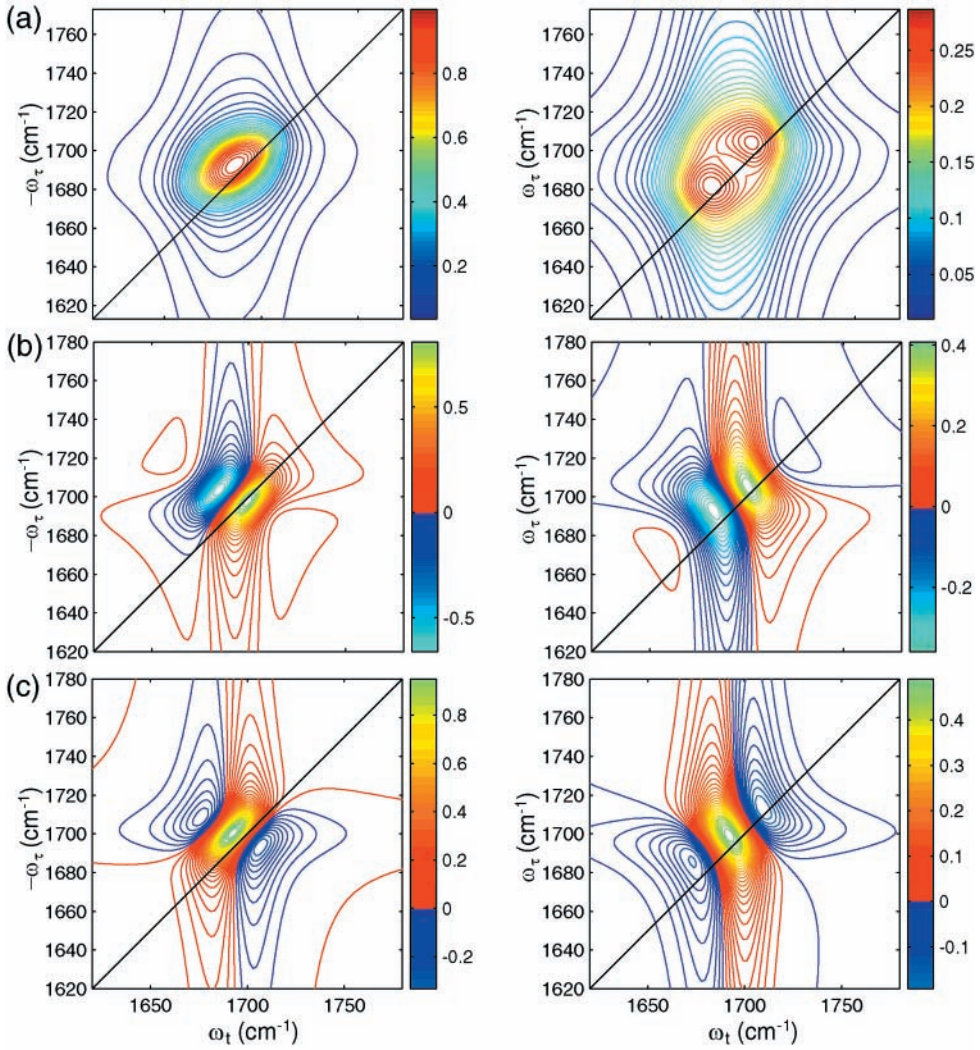

Figure 6. Calculated absolute value 2D spectra for two independent vibrators (a) at $\omega_i^0 = 1700$ cm^{-1} and $\omega_j^0 = 1686$ cm^{-1} with identical dynamical parameters $\Gamma_i = 6.4$ cm^{-1}, $\sigma_i = 6.0$ cm^{-1}, and $f_i = 0$. The real and imaginary 2D spectra for the vibrator at $\omega_i^0 = 1700$ cm^{-1} are shown in b and c. Left: rephasing spectra. Right: nonrephasing spectra.

remain unchanged. For some small molecules, the coupling can be directly obtained from the conventional anharmonic coupling parameters.[33,34]

Effects of Spectral Diffusion

Up until now, we have assumed that the system dynamics follow the Bloch model. In reality, this is not always the case. In fact, there are a number of known systems where spectral diffusion takes place.[24,25,35] The inhomogeneous distributions become time dependent and can be included in the line shape functions $g_{ii}(t)$, $g_{\Delta_i\Delta_i}(t)$, $g_{i\Delta_i}(t)$, and $g_{ij}(t)$. For example, if the frequency autocorrelation function for vibrator i can be written as $\langle\delta\omega_i(t)\delta\omega_i(0)\rangle = A_i^2 \exp(-t/\tau_i)$, then the line shape function becomes $g_{ii}(t) = A_i^2\tau_i^2(e^{-t/\tau_i} + t/\tau_i - 1)$. This is the Kubo model for spectral diffusion. The homogeneous and inhomogeneous limits are recovered by this model by setting $A_i\tau_i \ll 1$ and $A_i\tau_i \gg 1$, respectively. Another approach is to express the frequency autocorrelation function as sum of exponentials. It has been shown that a correlation function of this form provides good agreement with the experimental three pulse photon echo data for several single vibrator systems[24,25] assuming no fluctuation in the anharmonicity ($\sigma_{\Delta_i} = 0$). In principle, the autocorrelation functions $\langle\delta\Delta_i(t)\delta\Delta_i(0)\rangle$ could also be written as sum of exponentials. The cross-correlation functions $\langle\delta\omega_i(t)\delta\Delta_i(0)\rangle$ and $\langle\delta\omega_i(t)\delta\omega_j(0)\rangle$ will depend on the correlation coefficients f_i and c_{ij}, respectively. Once the forms of the correlation functions are determined, the calculation of the line shape functions and hence the response functions are straightforward.

Experimental Verification of the Differences between Spectra in the Rephasing and Nonrephasing Regimes

In this section, it is shown that the 2D IR spectra can be obtained in the different quadrants by using the two different pulse sequences discussed above. The differences between these two spectra are quite apparent.

Methods. Details of the laser system[36] and experimental setup[2,4] have been published previously and are only briefly described here. Tunable femtosecond IR pulses (duration 120 fs, bandwidth 150 cm^{-1}, repetition rate 1 kHz) were split into three equal excitation beams (~300 nJ each) and a fourth LO beam (~3 nJ). In our setup, the pulses k_1, k_3, and LO traversed computer-controlled optical delay stages, whereas the pulse k_2 was held fixed in time. Experiments were done with $T = 0$. When taking data for rephasing pathways, the stepping motor for pulse k_3 were held fixed at zero time delay with respect to k_2, and pulse k_1 was moved by τ preceding k_2 and k_3. When taking data for nonrephasing pathways, both stepping motors for pulses k_1 and k_3 were moved by the same τ delay with respect to k_2. The photon echo field emitted in the $-k_1 + k_2 + k_3$

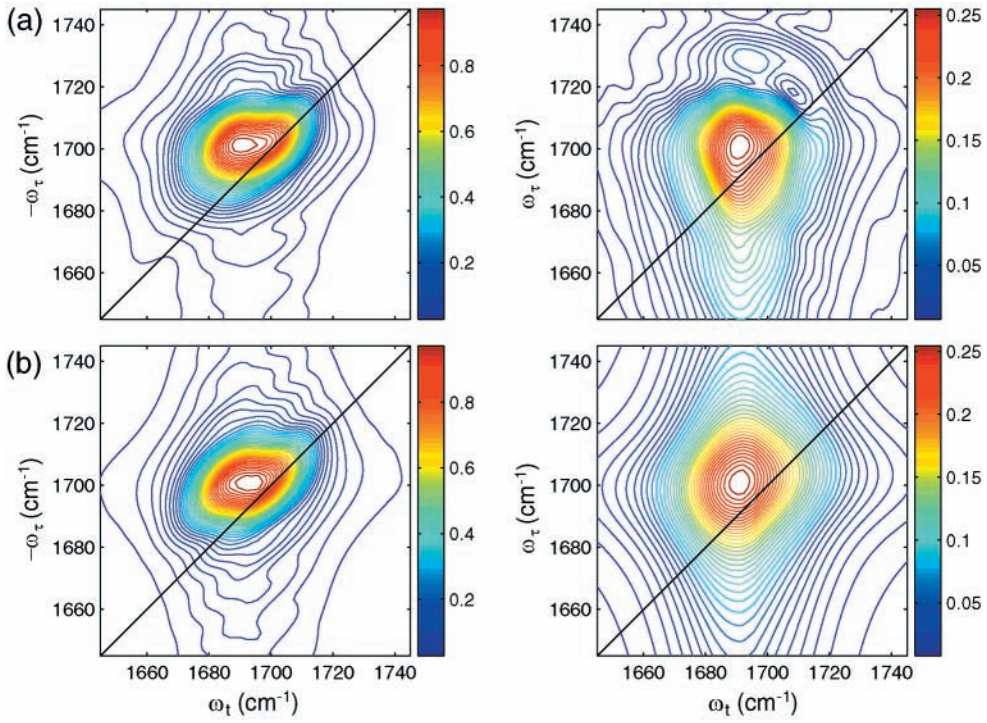

Figure 7. Experimental (a) and calculated (b) absolute value 2D spectra for 300 mM acetone in ethylene glycol. Left: rephasing spectra. Right: nonrephasing spectra. The parameters for the calculated spectra are discussed in the text.

direction was overlapped with the LO pulse and collected on a HgCdTe detector. In both cases, the LO pulse was always set to arrive after the pulse k_3, i.e., for every τ, the LO pulse is delayed with respect to k_2 by t and $\tau + t$ for rephasing and nonrephasing pathways, respectively. For experiments on acetone in ethylene glycol, τ was scanned from 0 to 2500 fs and t was scanned from 0 to 3500 fs. For experiments on acetylproline-ND_2 in D_2O, τ and t were scanned from 0 to 1600 fs. Before taking the Fourier transform, data points from 0 to 100 fs in τ were removed to eliminate contributions from diagrams around $\tau = 0$ (diagrams 7−8 of Figure 1). To reduce the data collection time, all scans were undersampled in steps of 18 fs and averaged for 25 and 40 shots for the rephasing and nonrephasing signals, respectively, at each data point. The plotted frequency axes were converted from the aliased frequency by adding the spectral width (inverse of sampling interval or two times the Nyquist frequency). All spectra are outputs from the Fourier transform of raw time domain data without applying any window functions. All experiments were conducted at room temperature.

HPLC grade acetone was purchased from Fisher Scientific and dissolved in ethylene glycol to give a 300 mM solution. Acetylproline-NH_2 was used as received from BACHEM and dissolved in D_2O to give a 150 mM solution. In D_2O, acetylproline-NH_2 deuterates to acetylproline-ND_2.

Experimental Results. Acetone dissolved in ethylene glycol serves as a model for a single vibrator system as discussed in Figure 3. In the linear-IR spectrum, the absorption peak of C═O stretch fundamental is centered at 1704.7 cm^{-1}. Fitting the line shape by a Voigt profile gives a 10.7 cm^{-1} Lorentzian width and an 11.1 cm^{-1} Gaussian width. The anharmonicity cannot be measured directly from the linear-IR spectrum because the overtone overlaps with the OH stretch vibrations of the solvent but is expected to be about 16 cm^{-1} as determined from the linear-IR spectra of acetone liquid and acetone in CCl_4 solutions. Figure 7a shows the experimental absolute value 2D IR spectra for the rephasing and nonrephasing pathways.

The second system is a dipeptide acetylproline-ND_2 in D_2O that serves as a model system containing two coupled amide I vibrators. The linear-IR spectrum shows two peaks. One at 1608.5 cm^{-1} corresponds to the acetyl end of the dipeptide, and the other at 1650 cm^{-1} corresponds to the amino end. The experimental absolute value 2D spectra are shown in Figure 8. The rephasing spectrum is consistent with the previous 2D IR measurements.[4]

Discussion

The rephasing spectrum of acetone in ethylene glycol [Figure 7a] is elongated along the diagonal, indicating line narrowing, whereas the nonrephasing spectrum is four times less intense and not elongated. These are characteristics of inhomogeneous broadening. Because ethylene glycol is a viscous solvent, it is expected that the C═O stretching mode of acetone molecules may sample different solvent environments that fluctuate on a slower time scale than vibrational dephasing, thus, giving rise to inhomogeneous broadening. The peak maxima in the rephasing and nonrephasing spectra in Figure 7a are both located closer to the anharmonically shifted 1−2 transition frequency than to the fundamental frequency in the ω_t direction.[37] Figure 7b shows a global fit to the experimental 2D spectra assuming the system follows Bloch dynamics and $(T_1{}^{i+i})^{-1} = 2(T_1{}^{i})^{-1}$. The overall line shapes are well reproduced with these parameters: $\omega_i^0 = 1701.6$ cm^{-1}, $\Delta_i^0 = 16.7$ cm^{-1}, $\Gamma_i = 2.8$ cm^{-1}, $\sigma_i = 7.1$ cm^{-1}, and $T_1{}^{i} = 6$ ps. Although parameters σ_{Δ_i} and f_i can take different combinations that give almost equally good fits, a general trend can be found. When the correlation is large, say $|f_i| > 0.95$, the corresponding σ_{Δ_i} is small (<0.3 cm^{-1}), but when the correlation is small, say $|f_i| < 0.5$, the corresponding σ_{Δ_i} can vary a wide range from 0.02 to 2.5 cm^{-1}. This behavior suggests that either one or both of the parameters σ_{Δ_i} and f_i are small for acetone in ethylene glycol, so that 2D line shape is sensitive to certain combinations of σ_{Δ_i} and f_i but not sensitive to the individual values. Although this is the case for this

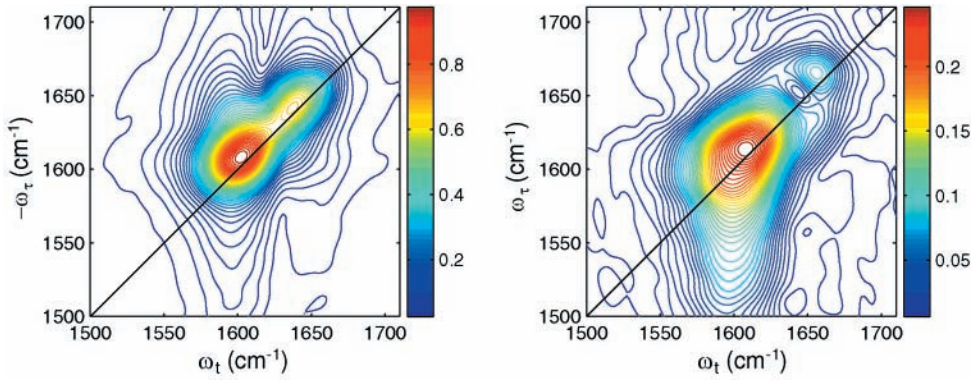

Figure 8. Experimental absolute value 2D spectra for 150 mM acetyl-proline-ND_2 in D_2O. Left: rephasing spectrum. Right: nonrephasing spectrum.

particular system, there may exist other systems that exhibit large values of σ_{Δ_i} and f_i, and a unique determination of individual parameters could become possible. We emphasize here the significant differences between the spectra in the two quadrants.

The rephasing spectrum of acetylproline-ND_2 (Figure 8) reproduces the spectral features found in the previous work:[4] there are two peaks elongated along the diagonal and a cross-peak above the diagonal [$(-\omega_\tau)>\omega_t$]. The high and low-frequency diagonal peaks correspond to the amino and acetyl amide I bands, respectively. As expected the nonrephasing spectrum (Figure 8) provides additional information. For example, the amino amide I band in the nonrephasing spectrum appears at a much higher frequency than the amino amide I band in the rephasing spectrum. In addition, a valley appears near $(\omega_\tau,\omega_t) = (1650,1650)$ in the nonrephasing spectrum that falls within the amino amide I peak in the rephasing spectrum. This behavior is similar to the calculated spectra shown in Figure 6a. This result suggests that there are actually two conformations whose amino amide I frequencies are separated by less than the line width and whose acetyl amide I frequencies are almost identical so that there is a valley in the amino amide I region but no valley in the acetyl amide I region. Interestingly, the experimental and theoretical studies of a similar dipeptide acetylproline-$NHCH_3$ found that it adopts α-helical (α_R) and extended (P_{II}) conformations in polar solvents.[38] Force field calculations and normal-mode analysis on acetylproline-ND_2 show that the frequency difference between the α_R and P_{II} conformations is 1 cm^{-1} for the acetyl amide I band and 13 cm^{-1} for the amino amide I band.[4] These findings are consistent with our results. Therefore, these results show that important information on conformational distributions of the system, not readily available from the linear-IR spectrum or from the 2D IR spectra in only one quadrant, can be obtained by measuring the nonrephasing 2D IR spectrum in conjunction with rephasing spectrum.

A slightly different experiment that will also exhibit the effects of correlation is the spectrum of the photon echo. In this experiment, the square of each Fourier component of the echo signal is obtained, i.e., $|E(\omega_t;\tau,T)|^2$. This signal is readily computed from the response functions given above. Previous spectrally resolved three pulse photon echo studies of the azide ion and hemoglobin C═O have investigated the effects of σ_{Δ_i}, f_i, and T_1^{i+i}.[18] It was concluded that σ_{Δ_i} is negligible for hemoglobin, assuming that T_1^{i+i} follows a harmonic model. A recent spectrally resolved two pulse photon echo study on a metal carbonyl also assumed $\sigma_{\Delta_i} = 0$.[26] However, these measurements were carried out only for the rephasing pathways. It is expected that measurements of spectrally resolved echoes for the nonrephasing pathways as well will provide additional information on correlations similar to that from heterodyned 2D measurements even though the spectra are not strictly line narrowed.

In principle, pump−probe experiments should also contain information on correlations. Although the nonrephasing pathways cannot be separated from the rephasing pathways because the first two pulses are indistinguishable from one another in pump−probe methods, the effects of correlations between vibrators can manifest themselves in the T period when the interstate coherences are evolving. Previous pump−probe self-heterodyned 2D experiments on a small globular peptide showed beating patterns in the time traces along T for several probe frequencies.[14] These oscillations gave rise to cross-peaks appearing at $\omega_T = |\omega_i^0 - \omega_j^0|$ in the 2D spectra of ω_T versus probe frequency. It was found that these cross-peaks are elongated along the probe frequency axis, indicating that the inhomogeneous distributions of these bands are positively correlated so that the fluctuations in ω_i^0 and ω_j^0 do not much affect the difference between them. It is expected from our results that other forms of correlation would result in a different shape of elongation. Similar effects are expected to appear in heterodyned transient grating 2D spectra as well. These effects can be readily simulated by eqs 5−12 along with (1) and (2).

In 2D NMR, rephasing and nonrephasing complex 2D spectra are often added or subtracted to obtain pure absorption or dispersion spectra.[1] Recent optical 2D studies employed similar concept in their data collection and treatment[10,39] In principle, adding IR rephasing and nonrephasing real spectra together would yield a 2D spectrum similar to that obtained from dynamic hole burning experiments [12,13] which incorporates a range of τ determined by the pump pulse (and hence includes contributions from diagrams 7 and 8 of Figure 1). Although the effects of frequency correlations remain in the combined spectrum, in our view, separated rephasing and nonrephasing complex spectra can make the information content of the spectra more evident than in combined spectra.

Conclusions

The effects of vibrational frequency correlations on heterodyned 2D IR spectra have been examined. Response functions were evaluated that will be useful in many different types of nonlinear-infrared spectroscopy. The line narrowing properties of 2D IR spectroscopy were analyzed qualitatively by a simple model and then quantitatively by numerical simulations using nonlinear response functions that include fluctuations of vibrational frequency, anharmonicity, and coupling between vibrators. For multilevel systems, echoes can also occur in the nonrephasing pathways if there exists some anticorrelation between the

relevant inhomogeneous frequency distributions. This is in contrast to the traditional picture of echoes which, we have emphasized, applies strictly only to two-level systems. In addition, closely spaced spectral features could exhibit more clearly resolved peaks in the nonrephasing quadrant than in the rephasing quadrant. Therefore, measuring 2D IR spectra in both quadrants separately is expected to significantly increase the information content obtained from photon echo experiments. As shown in the examples of acetone in ethylene glycol and acetylproline-ND_2 in D_2O, the measured rephasing and nonrephasing spectra are indeed quite different. The 2D spectra of acetone in ethylene glycol exhibit characteristics of inhomogeneous broadening and are sensitive to the combination of the fluctuation of the anharmonicity and its correlation to the 0−1 transition frequency. The nonrephasing spectrum of acetylproline-ND_2 in D_2O provides new evidence for the existence of two conformations in the solution. Our results show that the heterodyned three pulse photon echo 2D IR method has significant potential not only for determining structures, structural dynamics, and distributions but also for revealing correlations between structural fluctuations associated with different vibrators in the coupled molecular network.

Acknowledgment. This research was supported by the National Science Foundation and the National Institutes of Health with instrumentation developed under NIH-RR13456. M.T.Z. acknowledges a NIH-NSRA fellowship (1 F32 GM20462-01).

References and Notes

(1) Ernst, R. R.; Bodenhausen, G.; Wokaun, A. *Principles of Nuclear Magnetic Resonance in One and Two Dimensions*; Oxford University Press: New York, 1987.

(2) Asplund, M. C.; Zanni, M. T.; Hochstrasser, R. M. *Proc. Natl. Acad. Sci. U.S.A.* **2000**, *97*, 8219−8224.

(3) Zanni, M. T.; Asplund, M. C.; Hochstrasser, R. M. *J. Chem. Phys.* **2001**, *114*, 4579−4590.

(4) Zanni, M. T.; Gnanakaran, S.; Stenger, J.; Hochstrasser, R. M. *J. Phys. Chem. B* **2001**, *105*, 6520.

(5) Golonzka, O.; Khalil, M.; Demirdoven, N.; Tokmakoff, A. *Phys. Rev. Lett.* **2001**, *86*, 2154−2157.

(6) Zhang, W. M.; Chernyak, V.; Mukamel, S. *J. Chem. Phys.* **1999**, *110*, 5011−5028.

(7) Gorcester, J.; Millhauser, G. L.; Freed, J. H. *Modern Pulsed and Continuous Wave Electron Spin Resonance*; Wiley: New York, 1990.

(8) Hanaishi, R.; Ohba, Y.; Akiyama, K.; Yamanchi, S.; Iwaizumi, M. *J. Chem. Phys.* **1995**, *103*, 4819−4822.

(9) van Doorslaer, S.; Schweiger, A. *Chem. Phys. Lett.* **1997**, *281*, 297−305.

(10) Hybl, J. D.; Albrecht, A. W.; Gallagher-Faeder, S. M.; Jonas, D. M. *Chem. Phys. Lett.* **1998**, *297*, 307−313.

(11) Astinov, V.; Kubarych, K. J.; Milne, C. J.; Miller, R. J. D. *Chem. Phys. Lett.* **2000**, *327*, 334−342.

(12) Hamm, P.; Lim, M. H.; Hochstrasser, R. M. *J. Phys. Chem. B* **1998**, *102*, 6123−6138.

(13) Woutersen, S.; Hamm, P. *J. Phys. Chem. B* **2000**, *104*, 11316−11320.

(14) Hamm, P.; Lim, M.; DeGrado, W. F.; Hochstrasser, R. M. *J. Chem. Phys.* **2000**, *112*, 1907−1916.

(15) Likforman, J.-P.; Joffre, M.; Thierry-Mieg, V. *Opt. Lett.* **1997**, *22*, 1104−1106.

(16) See, for example: Joo, T. H.; Jia, Y. W.; Yu, J. Y.; Lang, M. J.; Fleming, G. R. *J. Chem. Phys.* **1996**, *104*, 6089−6108.

(17) Dick, B.; Hochstrasser, R. M. *J. Chem. Phys.* **1983**, *78*, 3398−3409.

(18) Asplund, M. C.; Lim, M.; Hochstrasser, R. M. *Chem. Phys. Lett.* **2000**, *323*, 269−277. There are some misprints in this paper that have been corrected in an erratum.[19]

(19) Asplund, M. C.; Lim, M.; Hochstrasser, R. M. *Chem. Phys. Lett.* **2001**, *340*, 611.

(20) Mukamel, S. *Principles of nonlinear spectroscopy*; Oxford University Press: New York, 1995.

(21) Hochstrasser, R. M. *Chem. Phys.* **2001**, *266*, 273−284.

(22) Kubo, R. *Adv. Chem. Phys.* **1969**, *15*, 101−127.

(23) Zimdars, D.; Tokmakoff, A.; Chen, S.; Greenfield, S. R.; Fayer, M. D.; Smith, T. I.; Schwettman, H. A. *Phys. Rev. Lett.* **1993**, *70*, 2718−2721.

(24) Hamm, P.; Lim, M.; Hochstrasser, R. M. *Phys. Rev. Lett.* **1998**, *81*, 5326−5329.

(25) Lim, M. H.; Hamm, P.; Hochstrasser, R. M. *Proc. Natl. Acad. Sci. U.S.A.* **1998**, *95*, 15315−15320.

(26) Merchant, K. A.; Thompson, D. E.; Fayer, M. D. *Phys. Rev. Lett.* **2001**, *86*, 3899−3902.

(27) Sahini, V. E.; Olteneanu, M. *Rev. Roum. Chim.* **1973**, *18*, 361−365.

(28) Misra, P.; Zhu, X. M.; Hsueh, C. Y.; Halpern, J. B. *Chem. Phys.* **1993**, *178*, 377−385.

(29) Chiang, S. Y.; Hsu, Y. C.; Lee, Y. P. *J. Chem. Phys.* **1989**, *90*, 81−86.

(30) Bevan, J. W.; Martineau, B.; Sandorfy, C. *Can. J. Chem.* **1979**, *57*, 1341−1349.

(31) Gnanakaran, S.; Hochstrasser, R. M. *J. Am. Chem. Soc.* In press.

(32) Hamm, P.; Lim, M.; DeGrado, W. F.; Hochstrasser, R. M. *Proc. Natl. Acad. Sci. U.S.A.* **1999**, *96*, 2036−2041.

(33) Khalil, M.; Tokmakoff, A. *Chem. Phys.* **2001**, *266*, 213−230.

(34) Tominaga, K.; Maekawa, H. *Bull. Chem. Soc. Jpn.* **2001**, *74*, 279−286.

(35) Hamm, P.; Lim, M.; DeGrado, W. F.; Hochstrasser, R. M. *J. Phys. Chem. A* **1999**, *103*, 10049−10053.

(36) Hamm, P.; Hochstrasser, R. M. Structure and dynamics of proteins and peptides: femtosecond two-dimensional infrared spectroscopy. In *Ultrafast Infared and Raman Spectroscopy*; Fayer, M. D., Ed.; Marcel Dekker, Inc.: New York, 2001; pp 273−347.

(37) This is in part due to the higher optical density of the sample at the fundamental frequency than at the 1−2 transition frequency, giving rise to stronger attenuation of the echo field at the fundamental frequency during its growth over the length of the sample.

(38) Madison, V.; Kopple, K. D. *J. Am. Chem. Soc.* **1980**, *102*, 4855−4863.

(39) Gallagher-Faeder, S. M.; Jonas, D. M. *J. Phys. Chem. A* **1999**, *103*, 10489−10505.